PASJ: Publ. Astron. Soc. Japan **60**, 991–999, 2008 October 25

SiO Maser Observations toward Orion-KL with VERA

Mi Kyoung KIM,[1] Tomoya HIROTA,[2,5] Mareki HONMA,[2,5] Hideyuki KOBAYASHI,[1,4] Takeshi BUSHIMATA,[3,5] Yoon Kyung CHOI,[4] Hiroshi IMAI,[6] Kenzaburo IWADATE,[4] Takaaki JIKE,[4] Seiji KAMENO,[6] Osamu KAMEYA,[4] Ryuichi KAMOHARA,[5] Yukitoshi KAN-YA,[9] Noriyuki KAWAGUCHI,[2,3,5] Seisuke KUJI,[4] Tomoharu KURAYAMA,[9] Seiji MANABE,[2,4] Makoto MATSUI,[8] Naoko MATSUMOTO,[2] Takeshi MIYAJI,[3,5] Takumi NAGAYAMA,[8] Akiharu NAKAGAWA,[6] Chung Sik OH,[1] Toshihiro OMODAKA,[6] Tomoaki OYAMA,[5] Satoshi SAKAI,[4] Tetsuo SASAO,[9] Katsuhisa SATO,[4] Mayumi SATO,[1] Katsunori M. SHIBATA,[2,3,5] Yoshiaki TAMURA,[2,4] and Kazuyoshi YAMASHITA[2]

[1]*Department of Astronomy, Graduate School of Science, The University of Tokyo, 7-3-1 Hongo, Bunkyo-ku, Tokyo 113-0033*
[2]*Department of Astronomical Sciences, Graduate University for Advanced Studies, 2-21-1 Osawa, Mitaka, Tokyo 181-8588*
[3]*Space VLBI Project, National Astronomical Observatory of Japan, 2-21-1 Osawa, Mitaka, Tokyo 181-8588*
[4]*Mizusawa VERA Observatory, National Astronomical Observatory of Japan, 2-12 Hoshigaoka, Mizusawa-ku, Oshu-shi, Iwate 023-0861*
[5]*Mizusawa VERA Observatory, National Astronomical Observatory of Japan, 2-21-1 Osawa, Mitaka, Tokyo 181-8588*
[6]*Faculty of Science, Kagoshima University, 1-21-35 Korimoto, Kagoshima, Kagoshima 890-0065*
[7]*Department of Astronomy, Yonsei University, 134 Shinchon-dong, Seodaemun-gu, Seoul 120-749, Republic of Korea*
[8]*Graduate School of Science and Engineering, Kagoshima University, 1-21-35 Korimoto, Kagoshima, Kagoshima 890-0065*
[9]*Korean VLBI Network, Korea Astronomy and Space Science Institute, P.O.Box 88, Yonsei University, 134 Shinchon-dong, Seodaemun-gu, Seoul 120-749, Republic of Korea*
mikyoung.kim@nao.ac.jp

(Received 2008 March 31; accepted 2008 September 1)

Abstract

We present results of phase-referencing VLBI observations of SiO masers in the Orion-KL region made with VERA. Using a strong maser spot in the 43 GHz $v = 2$ $J = 1$–0 emission, we derived the trigonometric parallax of Orion-KL to be 2.39 ± 0.03 mas, corresponding to a distance of 418 ± 6 pc, with the highest accuracy among existing parallax measurements of the source. We made a superimposed image of $v = 1$ $J = 1$–0 and $v = 2$ $J = 1$–0 maser features in Orion-KL based on absolute positions obtained from the phase-referencing astrometry with a common reference source. The maser features of both transitions show similar X-shaped distributions centered at Source I. However, in each of the four arms of the X-shape, the SiO $v = 2$ features tend to lie closer to Source I than the SiO $v = 1$ features. The radial velocities of the maser emission decrease with the distance from Source I. The spatial and radial velocity distributions of the SiO masers suggest that the SiO masers lie in the rotating materials associated with a disk around Source I, rather than a decelerating outflow.

Key words: astrometry — ISM: individual (Orion-KL) — masers (SiO)

1. Introduction

The Orion-BN/KL region is an ideal target for studying massive star formation because of its proximity and the existence of various masers, which allow us to trace the dynamics in the region with great spatial resolution. The "low-velocity" (or 18 km s^{-1}) flow and the "high-velocity" flow, centered at IRc 2, are detected in the Orion-KL region. The low-velocity flow extends northeast–southwest, and is recognized by tracing SiO, OH, and H_2O masers, as well as the thermal emission of several molecules (SiO, HCN, SO_2, SO). The high-velocity flow stretches in the northwest–southeast direction. This flow has been studied by the rotational transition of the CO molecule in the millimeter wave range (Genzel & Stutzki 1989). The Orion-BN/KL region is crowded with infrared sources, exhibiting ~ 20 compact peaks spread over $\sim 25''$ (Gezari et al. 1998). The BN object is the brightest near-IR source, but it contributes only a fraction of the total nebular luminosity of $\sim 10^5\,L_\odot$. IRc 2, giving rise to strong mid-IR emission, has been suspected to be the dominant energy source in the Orion-KL region since the centroid of CO emission lies within a few arcsecond of IRc 2, and the SiO molecule emission traces the high-velocity gas closest to the center. However, recent observations indicate that a compact radio continuum source, "I", which is offset from IRc 2, and is associated with SiO masers (Gezari 1992; Menten & Reid 1995), is a more likely center of activity.

Genzel et al. (1981) observed H_2O maser features in Orion-BN/KL using VLBI techniques and discussed three types of masers: low-velocity, high-velocity, and shell. The H_2O "shell" masers are distributed in a $2''$ by $0''.5$ strip oriented northeast–southwest, and are centered at Source I. The shell masers are clustered into two LSR velocity ranges: -8.2 to 1.0 km s^{-1} and 12.9 to 18.2 km s^{-1} (Gaume et al. 1998), and show expanding proper motions (Greenhill et al. 1998).

Source I displays strong SiO masers as well as H_2O masers.

SiO masers are usually detected in late-type stars, and are rare in the star-forming region. Only three star-forming regions contain a SiO maser: Orion-KL, W 51 IRS 2, and Sgr B2 MD5 (Morita et al. 1992). High-resolution observations for Orion-KL with VLA located Source I at the center of the SiO masers (Gezari 1992; Menten & Reid 1995). Early observations of 86 GHz SiO masers with the Hat Creek millimeter array showed that the SiO maser features in IRc 2 can be modeled by a simple expanding and rotating disk, whose rotation axis is in the northwest–southeast direction (Plambeck et al. 1990). The VLBA observations of Greenhill et al. (1998) revealed that the 43 GHz SiO masers are distributed in four regions that make X-pattern. SiO $v = 1$ and 2 $J = 1$–0 maser emission occur in two velocity ranges similar to that of a H_2O shell maser; the north and the west arms are red-shifted, while the south and east arms are blue-shifted. They suggested that the H_2O shell masers trace a thick, expanding disk (torus), and SiO masers trace a limb of an outflow oriented northwest–southwest that drives associated high-velocity outflow. Doeleman et al. (1999) also concluded that the SiO maser distribution indicates a bipolar outflow, although their explanation is different from that of Greenhill et al. (1998), in that Doeleman et al. (1999) considered the H_2O shell masers to outline a wide bipolar outflow as well as SiO masers, because both masers have the same velocity ranges.

In contrast, Greenhill et al. (2004) detected some maser features with the system velocity lying between the south arm and the east arm, which are referred to the "bridge". Moreover, they found that the relative proper motions of masers in the bridge are both outward and tangential. From these observations, they suggest that the SiO masers trace the limb of a bipolar outflow, probably the turbulent shocked interface between the disk of which axis is oriented northeast–southwest and the outflow which is perpendicular to the disk (e.g., Greenhill et al. 2004; Reid et al. 2007). If this model is correct, the SiO masers in Source I indicate strong evidence that the massive stars formed via accretion mediated by the disk. However, the model leaves an unknown driving source of high-velocity CO flows, and is inconsistent with the direction of the torus traced by OH masers (Cohen et al. 2006).

Source I is embedded in a molecular cloud behind the well-known H II region, M 42, and is coincident with a complex of infrared sources with $L_{\rm bol} \sim 10^4\ L_\odot$. Proper-motion measurements of Source I and BN suggest that they might have been part of a multiple system that disintegrated about 500 years ago (e.g., Rodríguez et al. 2005; Gomez et al. 2005). Some authors argue that it implies that Source I was formed by a merging event (e.g., Bally & Zinnecker 2005).

As described above, there are clearly different interpretations of the dynamical structure of the region around Source I among various authors (e.g., Bally & Zinnecker 2005; Greenhill et al. 2004), with assumed directions of the disk (torus) axis, or the outflow axis being offset by 90°, although they are based on essentially the same observational data. The motions of the SiO masers are explained by the outflow in one model, and by rotation of the matter at the rotating disk (torus)-outflow interface in another. To distinguish between these two models, it is essential to accurately measure the absolute positions and the absolute proper motions of the SiO maser features using phase-referencing observation with high resolution.

With this in mind, we conducted VERA observations of Orion-KL to measure the absolute positions and the proper motions of SiO masers, and to constrain the model of the structures and dynamics of the gas surrounding Source I. In this paper, we report on a trigonometric parallax measurement with high accuracy using SiO maser emissions. In addition, we present the results of measurements of the absolute positions of the $v = 1$ and 2 $J = 1$–0 SiO masers in the Orion KL region to register maps of the two transitions and to discuss the physical conditions in the masing region.

2. Observations and Data Analyses

Observations of the $v = 1$ $J = 1$–0 (43.122 GHz) and $v = 2$ $J = 1$–0 (42.821 GHz) transitions of SiO masers with VERA have been made since 2006 November, and here we present the data of 7 epochs. VERA, VLBI Exploration of Radio Astrometry, is a VLBI network in Japan which is dedicated to phase-referencing observations, and is aiming at a 10 microarcsecond accuracy of parallaxes and proper motions of masers (Kobayashi et al. 2008). VERA has four 20 m antennas, and each antenna is equipped with a dual-beam receiving system for 22 GHz and 43 GHz, which enables us to observe a target source and reference sources with a separation angle of 0.°3–2.°2 simultaneously (Kawaguchi et al. 2000; Honma et al. 2003). The maximum baseline length is 2270 km and the minimum baseline length is 1019 km. The interval of observations was about 1 month and the epochs are 2006/306, 2006/335, 2007/008, 2007/042, 2007/078, 2007/117, and 2007/151 (year/day of year). In each epoch, the observation was made for 8 hours.

In order to determine the absolute positions of the maser emissions, the target source, SiO masers in Orion-KL, and the reference source, J0541−0541, were observed simultaneously in the dual-beam mode. The tracking position for the target source was $(\alpha,\ \delta)_{\rm J2000.0} = (5^{\rm h}35^{\rm m}14\overset{\rm s}{.}505,\ -05°22'30\overset{''}{.}45)$, determined by Wright et al. (1990), and the position of the reference source was $(\alpha,\ \delta)_{\rm J2000.0} = (5^{\rm h}41^{\rm m}38\overset{\rm s}{.}083385,\ -05°41'49\overset{''}{.}42839)$ (Ma et al. 1998; Petrov et al. 2007). The separation angle between the target and the reference source is 1.°62. J0541−0541 was detected with a flux density of about 700 mJy beam^{-1} in all observations. A bright continuum source, J0530+1331, was observed every 1 hour for bandpass and delay calibrations.

The data were recorded on magnetic tapes at a rate of 1024 Mbps with the SONY DIR2000 recording system, which provided a total bandwidth of 256 MHz with 2-bit digitization. The 256 MHz bandwidth data were divided into 16 IF channels, and two of them were assigned for each SiO transition, while others were assigned for continuum emission from the reference source. The data were correlated with the Mitaka FX correlator. For the maser source, each IF channel was divided into 512 spectral channels, resulting in a velocity resolution of 0.21 km s^{-1}. The system temperatures were 200–700 K, depending on the weather condition and the elevation angle of the sources.

All data reductions were performed with the NRAO AIPS

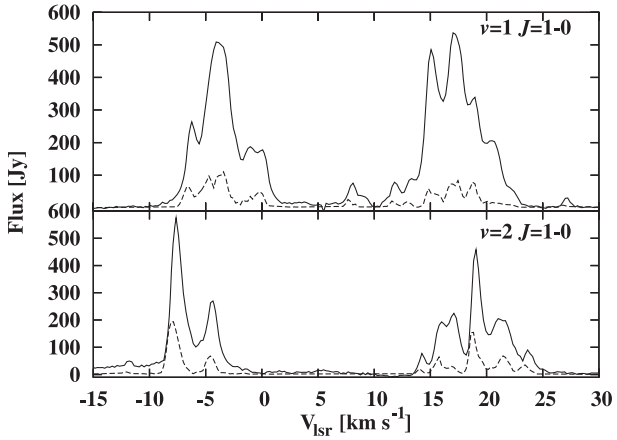

Fig. 1. Total power spectra in the Mizusawa station (a black line) and the integrated flux density of all features (a dashed line) on the map at 2007/117. The images of SiO masers by VERA recover $\sim$20% of the single-dish flux density.

software. At first, we carried out single-beam VLBI imaging for the target and the reference source independently to obtain maps of the overall distribution of the SiO maser features. In this paper, we define a maser "spot" as spatially isolated emission occurring in a single velocity channel and a "feature" as a sum of spots that are spatially coincident within the beam size, and are detected for at least two contiguous velocity channels. For the target source, a velocity channel in which only one bright spot exists were self-calibrated, the results of phase and amplitude calibrations were applied to other velocity channels. After the calibration process, we made images for each velocity channel using the AIPS task IMAGR to search for maser features. A signal-to-noise ratio, which is defined as the ratio of the peak flux to the rms noise level of each channel map, higher than 7 over at least two adjacent channels was adopted as the detection criteria for a maser feature. The rms noise level for channel maps was $\approx 0.3\,\mathrm{Jy\,beam^{-1}}$. Although the intensity of the highest sidelobe of a bright spot, which sometimes reaches about 10% of the peak intensity of the spot, may put a restriction for detecting a faint spot near a bright spot, we are certain that maser spots brighter than $\sim 2\,\mathrm{Jy\,beam^{-1}}$ are firmly detected. The number of detected features ranged from 30 to 80 and from 70 to 130 for the $v = 1$ and $v = 2$ transitions over the different epochs, respectively, due to varying observational conditions and variability of maser emissions. Figure 1 shows the total power spectrum in Mizusawa station and the integrated flux density of all features on the map at 2007/117. It shows that the images of SiO masers by VERA observations recover $\sim$20% of the single-dish flux density.

We then performed data reduction for dual-beam VLBI imaging. Amplitude calibration was done for the target (Orion-KL) and the reference source (J0541−05) independently. We determined the residual group delay and phase rate for the reference source using the AIPS task FRING, and the phase solutions were applied to the target (Orion-KL) for phase referencing. In addition, we applied the results of a dual-beam phase calibration to the target in order to calibrate the phase error caused by the difference of the signal path between two beams (Honma et al. 2007). After correcting for the Doppler shift due to Earth's motion, we made an image of a maser spot that is bright and compact using the AIPS task IMAGR. We measured the position of the maser spot from the reference source by fitting an elliptical Gaussian brightness distribution to the image using the AIPS task JMFIT. The typical synthesized beam size was 0.8 mas × 0.5 mas with a position angle of −30°.

3. Results

3.1. Annual Parallax

We measured the absolute positions for one bright maser spot during 7 epochs to obtain the trigonometric parallax of the Orion-KL region. We used one of the SiO $v = 2$ maser spots in the east arm of which V_{lsr} is $\sim 9\,\mathrm{km\,s^{-1}}$, detected in all of the 7 epochs. Since most of the maser emission, have a lifetime of $\lesssim$5 months, which is insufficient for estimating parallax, we could find the parallax for only one spot. In figure 2c, the positions of a maser spot in the sky during 7 epochs are shown. It is obvious that the movement of the maser spot is modulated into a sinusoidal pattern by the trigonometric parallax. Assuming that the movement of the maser spot is the sum of the linear motion and the parallax motion on the celestial sphere, we determined the initial position, proper motion, and trigonometric parallax by means of a least-squares analysis.

As a result of the fitting, we found the trigonometric parallax of the SiO maser around Source I to be 2.39 ± 0.04 mas using only right-ascension data and 2.44 ± 0.20 mas using only declination data. The fitting using both right-ascension and declination data yielded a result of 2.39 ± 0.03 mas. The linear proper motion of the spot determined by the fitting was $9.56 \pm 0.10\,\mathrm{mas\,yr^{-1}}$ and $-3.83 \pm 0.15\,\mathrm{mas\,yr^{-1}}$ in right ascension and declination, respectively. The derived annual parallax of 2.39 ± 0.03 mas corresponds to a distance of 418 ± 6 pc, with an uncertainty of only 1.5%.

The error bars in figure 2 were estimated from post-fit residuals assuming equal dispersion for all epochs. Their values, 40 μas for right ascension and 72 μas for declination, are much larger than the typical thermal noise error of 10 μas, suggesting systematic errors of our observation. In phase-referencing VLBI observations, the possible contributions to systematic errors are: (1) the airmass correction error, (2) the baseline length error, (3) the effect of the phase-reference source structure, (4) the structure any variation of the maser features (Hirota et al. 2007). Here, we discuss the possible errors in our observations by estimating these values. The airmass correction error is caused by differences in the optical path lengths for the target and phase-reference sources through the atmosphere because of a difference in the elevation angles (Honma et al. 2008). We roughly estimated a possible range of position errors due to the airmass effect during observations of our pair of sources, assuming 3 cm error in the zenith excess path length at all stations (Honma et al. 2007). The results showed that the airmass correction error is expected to be 40–80 μas, depending on the elevation angle of the source. We estimated the largest effect of the baseline error to be 5 μas for a separation angle of 1.°62, assuming a 3 mm error in the 1000 km baseline. The error caused by the phase-reference source structure

Table 1. Results of a least-squares analysis for the annual parallax and proper motion.

	ϖ [mas yr^{-1}]	D [pc]	$\Delta\alpha$ [mas]	$\Delta\delta$ [mas]	$\mu_\alpha \cos\delta$ [mas yr^{-1}]	μ_δ [mas yr^{-1}]
Right ascension	2.39(0.04)	418.7(6.4)	0.040	—	—	—
Declination	2.44(0.20)	409.5(33.8)	—	0.072	—	—
Right ascension & declination	2.39(0.03)	418.4(5.9)	0.040	0.072	9.56(0.10)	−3.83(0.15)

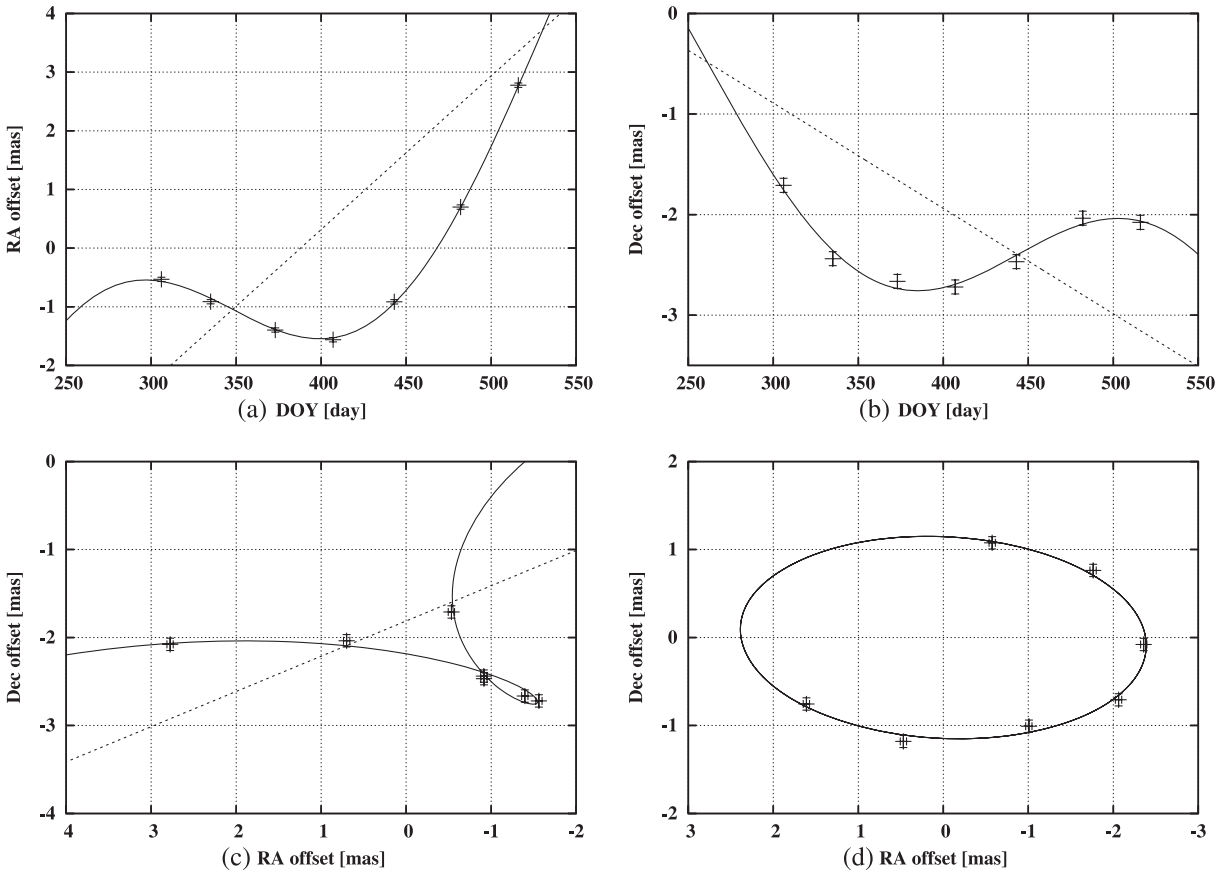

Fig. 2. (a) Movement of a maser spot in right ascension. (b) Movement in declination. (c) Motion of the spot in the sky during 7 epochs. (d) Ellipse represents the parallactic motion of the spot that the linear proper motion is subtracted. In these figures, a solid curve and a dashed line indicate the best-fit model with the sum of the annual parallax and linear proper motion and the linear proper motion only, respectively.

is calculated from the dynamic range of the phase-reference source's map. With a dynamic range of 60 on average, and a synthesized beam width of 0.8 mas, the error is less than 7 μas. The error caused by the structure of the phase-reference source would be negligible because the reference source had at a point-like structure in the images. The effect of the variation of the maser structure is suspected to be one of the major sources of systematic error in phase-referencing observations of a nearby H_2O maser source (e.g., Hirota et al. 2007, 2008; Imai et al. 2007). For instance, Hirota et al. (2007) argued that the structure of the H_2O maser feature in Orion-KL would be as large as 0.2 mas, which possibly degraded their astrometric accuracy. In contrast, the effect of the maser structure seems to be much less significant for our SiO maser observations in Orion-KL than that for the H_2O maser. Although the systematic velocity shift during 7 months and changes in the amplitude of the maser spot were confirmed by our observations, the maser feature displayed an unresolved source in the images, and the peak positions of the maser spots within the maser feature shifted by $\lesssim$0.05 mas from that of the adjacent channels, which is much less than a shift of about 0.2 mas shown in a H_2O maser observation by Hirota et al. (2007). Moreover, our residuals from the best-fit curves shown in figure 2 are much smaller and smoother that those obtained for the nearby H_2O masers.

In conclusion, the position uncertainty of 40 μas in right ascension and 72 μas in declination derived from least-squares fittings can be explained mainly by the airmass correction error with the estimated possible range of effect of 40–80 μas. The baseline error and the error caused by the phase-reference

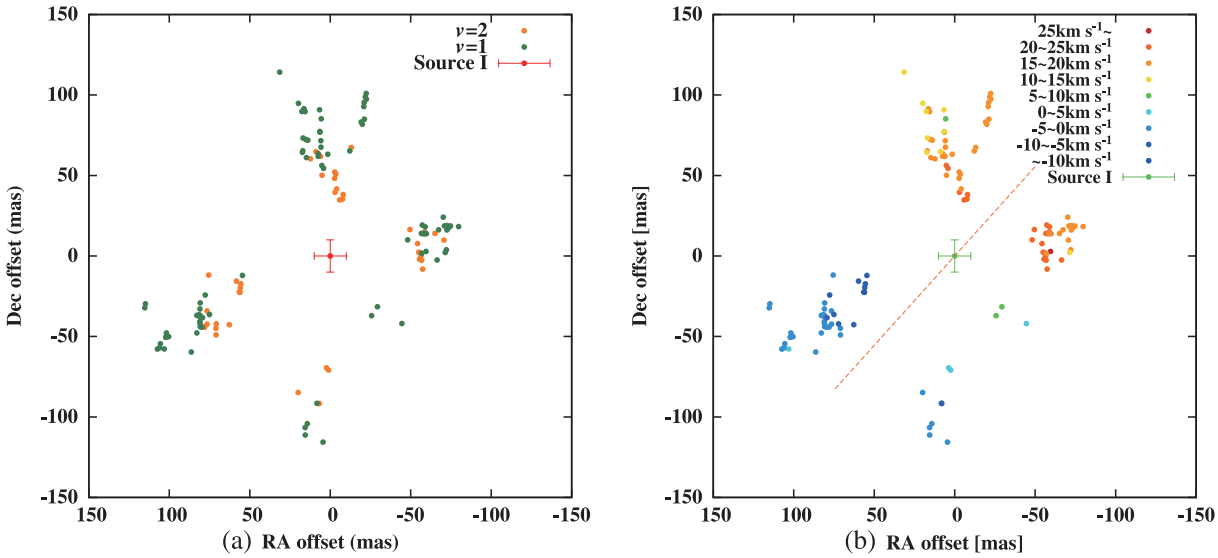

Fig. 3. Spatial and the radial velocity distribution of $v = 1$ and 2 $J = 1$–0 maser spots with respect to Source I in 2007/117. (0, 0) is the position of Source I in 2007/117, which is estimated by the proper motion of Source I and the position at 2002 March (Rodríguez et al. 2005). The size of cross corresponds to the positional error of 10 mas. (a) Yellow dots indicate $v = 2$ $J = 1$–0 transitions while the green dots indicate $v = 1$ $J = 1$–0 transitions. (b) Radial velocity distribution of $v = 1$ and 2 $J = 1$–0 maser features. The color represents the radial velocity of the features. The red dashed line indicates the major axis having an X-pattern.

source structure are much smaller than the estimated position uncertainty. Though we cannot the completely eliminate the maser structure effect, the fact that the estimated position uncertainty in declination is nearly twice as large as that in right ascension suggests the predominating role of the airmass correction error. In principle, it is expected that any statistical error will be reduced by a factor of $N^{-0.5}$ by estimating the parallax using many maser features, where N represents the number of maser features. We will confirm this expectation in further analyses of the VERA observations.

3.2. *Distributions of the SiO Masers*

Figure 3 shows the spatial distribution of SiO $v = 1$, 2 $J = 1$–0 masers based on the absolute positions with a precision of better than 1 mas (such an offset would be hardly seen on the scale of this figure). In this figure, the position of Source I is estimated with the position in 2002 March and the proper motion measured with VLA (Rodríguez et al. 2005). SiO masers are confined to four regions that make an X-like pattern centered on Source I, confirming previous results by VLBI observations (Greenhill et al. 1998; Doeleman et al. 1999). They are spread over a region with characteristic scales of 200 mas for the $v = 1$ transition and 150 mas for the $v = 2$ transition. The mean and the standard deviations of the distance of SiO $v = 1$ emissions from Source I are 35 ± 8 AU, and those of SiO $v = 2$ emissions are 26 ± 6 AU at 418 pc. Though their distributions partly overlap with each other, the mean distances from Source I differ by more than their standard deviations. Moreover, in figure 3a we can clearly see that there are regions in which only $v = 1$ features are located at the outer parts of all four arms of X-shape. Therefore, our result suggests that two transitions are distributed in regions with different distances from Source I. Such a clear offset in the spatial distributions of $v = 1$ and $v = 2$ masers is a distinct characteristic of the SiO masers in Orion-KL, which is not seen among circumstellar SiO masers around late-type stars.

In all epochs, except for 2007/151, we detected several maser features with a systemic velocity between the south arm and the west arm, which correspond to the "bridge" detected by Greenhill et al. (2004). Previous studies of multi-line observations reported that $v = 2$ $J = 1$–0 SiO masers are mainly distributed in this region (Greenhill et al. 2004), and that there are $v = 1$ $J = 2$–1 emission as well as $v = 1$ $J = 1$–0 emission (Doeleman et al. 2004). However, in our observations, all of the maser features in the bridge are $v = 1$ emission, in contrast to the result of Greenhill et al. (2004) that the bridge is outlined by $v = 2$ emission. The reasons for this difference could be: (1) the $v = 2$ bridge maser features are too weak for our image sensitivity, (2) the $v = 2$ bridge maser features are too extended and resolved out with the synthesized beam of VERA, and (3) the relative strengths of the $v = 1$ and $v = 2$ transitions were reversed during the interval between the VLBA and the VERA observations. We cannot specify at present the reason for non-detection, since we have no information about the flux or size of the bridge maser in VLBA observations. However, (1) and (2) are likely to contribute, at least partly, to our non-detection, because the $v = 1$ bridge masers detected in our observations are not very bright ($\lesssim 5\,\mathrm{Jy\,beam^{-1}}$), and there is no $v = 2$ emission of the system velocity in the total power spectrum in $v = 2$ emission (see figure 1).

Figure 3b gives a map of the radial velocity distribution of the maser features on 2007/117. The radial velocities of the maser features are roughly divided into two components: -13 to $1\,\mathrm{km\,s^{-1}}$ and 5 to $26\,\mathrm{km\,s^{-1}}$. The emission to the north-west is red-shifted, while that to the south-east is blue-shifted with respect to the systemic velocity of $\sim 5\,\mathrm{km\,s^{-1}}$, which is estimated by the mean velocity of the SiO masers (Plambeck et al. 1990). Figure 3b shows that the radial

velocities of the emission tend to decrease with the distance from Source I. Figure 4 gives a position–radial velocity diagram (P–V diagram) with the data from all 7 epochs. We confirmed the velocity gradient of $\sim 0.4\,\mathrm{km\,s^{-1}AU^{-1}}$ along the major axis of the X-pattern in both red-shifted and blue-shifted arms, as shown in figure 3b. The velocity gradient of maser emissions along the red-shifted arms has been reported by VLBA observations (e.g., Doeleman et al. 2004; Greenhill et al. 1998). Doeleman et al. (2004) observed a smooth velocity gradient of $\sim 0.5\,\mathrm{km\,s^{-1}}$ along the northern arm, and argued that the velocity gradient is due to an effect local to this region. Greenhill et al. (1998) also argued that only a red-shifted lobe shows a velocity gradient, and that three of four arms do not. The origin of this radial velocity distribution is discussed in a later section.

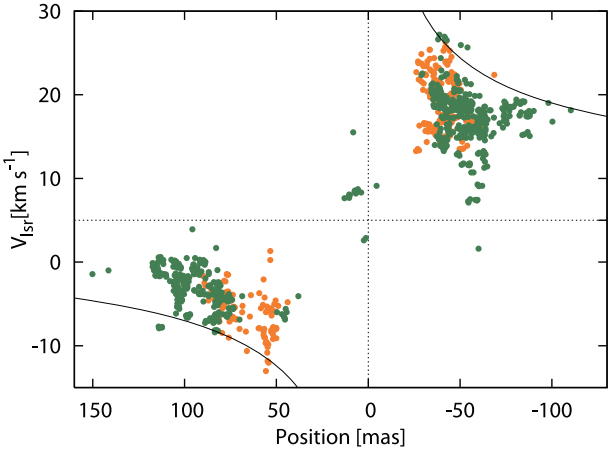

Fig. 4. Position–radial velocity diagram with data from all 7 epochs along the major axis of the X-pattern. The horizontal axis indicates the distance from Source I along the major axis of the X-pattern with a position angle of −48° (see figure 3b), which was determined by averaging the position angles of four arms. The color index is the same as an figure 3a. The dotted lines give the position and the radial velocity of the centroid, $5\,\mathrm{km\,s^{-1}}$. A Keplerian rotation curve for an $8\,M_\odot$ object is also plotted for a reference (solid line).

4. Discussion

4.1. Comparison with Other Distance Measurements

The most reliable way to conduct an astronomical distance measurement is the trigonometric parallax method, which is based on measurements of an absolute position and the motion of an object. Recently, the parallax measurements of Orion-KL with high astrometric accuracy are being achieved with VLBI techniques. Hirota et al. (2007) reported a distance of $437 \pm 19\,\mathrm{pc}$ from H_2O masers in Orion-KL using VERA. The observation of a non-thermal radio source, GMR A, using VLBA led to a distance estimation of $389^{+24}_{-21}\,\mathrm{pc}$ (Sandstrom et al. 2007) while a VLBA observations of three non-thermal radio sources, GMR A, GMR 12, GMR F, yielded the distance of $414 \pm 7\,\mathrm{pc}$ (Menten et al. 2007).

Our result from observations of SiO masers, $418 \pm 6\,\mathrm{pc}$, is consistent with the above results, and yields the distance with the highest accuracy. From our result as well as other trigonometric parallax observations, it is clear that the distance to the Orion Nebula is lower than the distance of 450 pc, which is often assumed for the Orion Nebula (Genzel & Stutzki 1989). Sandstrom et al. (2007) mentioned that there might be a large separation between the BN/KL and the Orion Nebula along the line of sight, comparing their VLBA result for distance of GMR A with the VERA result for Orion-KL by Hirota et al. (2007). However, our present result, $418 \pm 6\,\mathrm{pc}$ for Orion-KL, is very consistent with another VLBA result by Menten et al. (2007) with a higher quoted accuracy, $414 \pm 7\,\mathrm{pc}$. Thus, we can rule out the possibility of a large $\sim 30\,\mathrm{pc}$ line-of-sight separation between the BN/KL region and the Orion Nebula which are spread over $90'' \times 90''$ area in the sky, corresponding to only $0.2\,\mathrm{pc} \times 0.2\,\mathrm{pc}$ at a distance of 418 pc.

4.2. Kinematics of SiO Masers

In this paper, we determined the most accurate distance to Orion-KL with an uncertainty of only 1.5%, which allows us to refine the physical and dynamical properties of Orion-KL. Here, we discuss the physics and the dynamics of Orion-KL, in particular inferred from the distributions of the SiO maser features based on their phase-referenced images.

To explain the X-like pattern and the double-peak velocity distribution, two dynamical models for SiO masers have been proposed, as discussed in the Introduction: an outflow oriented to a northwest–southeast and a disk with northeast–southwest rotation axis. We now discuss the possibility of each model. First of all, our P–V diagram (see figure 4) clearly confirms a decline of the radial velocity with the distance from Source I in both red- and blue-shifted regions. In the case of the outflow model, the velocity gradient of maser emissions should be explained by a deceleration in the line-of-sight component of the outflow velocity. The outflow velocity traced by the SiO masers must be larger than the escape velocity, which is $v_{\mathrm{esc}} \sim (2GM/r)^{1/2} \sim 23$–$29\,\mathrm{km\,s^{-1}}$ at 20 AU and for possible mass ranges of the central star, $M = 6$–$10\,M_\odot$. However, our observation shows that the radial velocities are less than $20\,\mathrm{km\,s^{-1}}$ at 20 AU. Assuming the proper motion of the maser to be $\sim 10\,\mathrm{km\,s^{-1}}$ (Greenhill et al. 2004), the velocities of the maser features at 20 AU are $\lesssim 22\,\mathrm{km\,s^{-1}}$. Thus, it is expected that matters are pulled down to the central star by gravitation. This is a rather severe constraint against the simple decelerating outflow model. Moreover, in simple decelerating outflow, the transverse velocity is also expected to decelerate as a function of the distance from the central star. However, the relative proper motions reported by Greenhill et al. (2004) show no dependence on the distance, contrary to the prediction.

On the other hand, the velocity gradient along the projected axis would be accounted for by a differential rotation. In this case, SiO masers might trace the upper- and lower side of a thick, rotating disk. Assuming simple Keplerian rotation, we can calculate the inner mass, M, at a radius of r by $M \sim v^2 r/G$, where G is the gravitational constant, and v is velocity at radius r. With a radius of ~ 42 AU and a velocity of $\sim 12\,\mathrm{km\,s^{-1}}$, we can estimate M to be $8/(\sin i)^2\,M_\odot$, where i is the inclination angle between the disk axis and the celestial sphere. We consider that the inclination angle of the disk is $\sim 90°$, because the X-pattern of the masers is almost symmetrical. The mass of $8\,M_\odot$ is practically consistent with the mass of Source I $> 6\,M_\odot$, estimated by a VLBA observation

and $\sim 10\,M_\odot$ estimated by a 43 GHz continuum the observation (e.g., Reid et al. 2007; Greenhill et al. 2004). However, observed radial velocities of masers is lower than the expected velocity profile of Keplerian rotation for an $8\,M_\odot$ protostar (see figure 4). Moreover, the velocity profile from our observation tends to be flatter in the outer region than the curve that is expected with a $v \sim r^{-0.5}$ tendency. Thus, it is likely that a non-Keplerian rotation would contribute to the observed velocity structure. Reid et al. (2007) found an elongated continuum emission centered on Source I in 43 GHz continuum observations. The emission spreads over the same spatial range with SiO masers, and can be modeled by an edge-on ionized disk with a mass of $\sim 3\,M_\odot$. Compared to the estimated mass of the protostar/disk system of $\sim 8\,M_\odot$, the mass of the disk is considerable. Hence, a Keplerian rotation disk, assuming that the disk mass is negligible compared to the mass of the central star, would not be feasible in this system. Furthermore, the expanding proper motions of masers (Greenhill et al. 2004) are indicative of non-Keplerian rotation. The expanding motion suggests that there are some additional forces against gravitation (for instance, a stellar wind or radiation pressure) other than the centrifugal force. These outward forces could make the effects of gravitation to be underestimated.

In this case, H_2O shell masers, which are distributed along the northeast–southwest axis, is perpendicular to the disk, and may trace outflow with no inclination because each lobe of a bow-tie has a double-peak spectrum over the same velocity ranges with each other. Its velocity range is almost the same as that of SiO masers (Gaume et al. 1998), despite the fact that the spatial distribution of H_2O masers is one order of magnitude wider than that of SiO masers. The result of Gaume et al. (1998) shows that H_2O masers have a similar velocity distribution as SiO masers in the region close to Source I, although the velocity gradient of H_2O masers is not as clear as that of SiO masers. In the more distant region, however, red- and blue-shifted components are mingled and the velocity range of masers in this region is wider than that in the region close to Source I. The velocity distributions suggest that H_2O masers nearby SiO masers are excited in the boundary between the outflow and the disk, and thus, the velocity distribution is aligned in the same manner as the SiO masers. In the more distant region, H_2O masers might be in the interacting region between the outflow and the ambient matter. According to above discussions, we suggest that the rotating disk model is more likely to account for the spatial and radial velocity distributions of the SiO masers in Orion-KL. However, more thorough modeling based on the 3-D velocity field of the maser features, and further observations are needed to inspect the feasibility of this model.

4.3. *Maser Pumping*

As a result of our astrometric observation, we succeeded to superimpose maps of two transitions, and found that there is a distinct positional offset between the $v = 1, 2$ emissions. The distributions of emissions from the different vibrational transitions can reveal a small-scale physical condition of the masing region and the pumping mechanisms. Our result shows that SiO $v = 1$ emissions lie around a mean radius of 35 ± 8 AU, and SiO $v = 2$ emissions lie around a radius of 26 ± 6 AU from Source I at the 418 pc distance, and that two transitions are considerably offset. Matthews et al. (2007) suggested that $v = 2$ masers tend to lie closer to Source I than do $v = 1$ masers, but there are considerable overlaps. In late-type stars, SiO masers are located in the upper parts of the stellar atmosphere (Elitzur 1980). Radiative and collisional pumping mechanisms are suggested to explain SiO masers. Miyoshi et al. (1994) showed that the $v = 1,\ 2$ $J = 1$–0 SiO masers in VY CMa are coincident within 2 mas, and explained this by a collisional pumping mechanism. However, Bujarrabal (1994) suggested that the line overlap effect between a vibrational transition of H_2O and SiO may introduce a coincidence between the $v = 1$ and $v = 2$ $J = 1$–0 transitions even in the radiative pumping scheme. Moreover, in recent high-resolution observations, it is shown that $v = 2$ masers lie closer to the central object than $v = 1$ masers, as an expectation based on the excitation temperatures. Soria-Ruiz (2005) found that the $v = 1$ and $v = 2$ $J = 1$–0 transitions show a similar spatial distribution, and the $v = 2$ emission is located in a slightly more inner region than the $v = 1$ emission in AGB stars. Yi et al. (2005) also discussed that the $v = 2$ $J = 1$–0 masers are slightly closer to the star than the $v = 1$ $J = 1$–0 masers in TX Cam. Nevertheless, this is rare even in late-type stars that the two transitions are separated by a considerable offset.

The number of existing pumping models for SiO masers in Orion-KL is rather limited. Elitzur (1982) constructed a model for SiO masers in Orion-KL with the assumption of spherical expansion, and concluded that the masers are pumped by collisions in the region where an outflow is established as a result of radiation pressure on newly formed dust. However, this model could not give a good explanation because spherical symmetry is assumed, which is contrary to the observed outflow/disk. Meanwhile, Deguchi and Nguyen-Quang-Rieu (1983) reported that SiO masers in Orion-KL are radiatively pumped by 8 μm photons emitted by a thin dust shell heated by shock waves. To achieve a strong inversion, gas density must be as high as $\sim 10^{10}\,\mathrm{cm}^3$ and the masers occur at a radius of 3×10^{14} cm, close to the stellar photosphere. The estimated range of the masing region is consistent with the observation, but the distributions of the $v = 1$ and 2 transitions are not discussed. Moreover, the radiation field of the central star has to be considered for a more detailed model. Zeng et al. (1987) constructed a model for SiO emissions in Orion-KL and selected the optimum parameters by solving the statistical equilibrium and radiative transfer equations. They assumed that a spherical expanding shell is exposed to radiation from the central star with a luminosity of 10^4–$10^5\,L_\odot$ and a high mass-loss rate. The result of a model calculation with a set of parameters gives that $v = 1, 2$ masers lie in a shell of kinetic temperature $1200\,\mathrm{K} < T_\mathrm{k} < 1500\,\mathrm{K}$ and density $4 \times 10^9 \mathrm{cm}^3 < n(\mathrm{H_2}) < 4 \times 10^{10} \mathrm{cm}^3$ when dust temperature $T_\mathrm{d} \sim 550\,\mathrm{K}$. At the higher dust temperature $T_\mathrm{d} \sim 700\,\mathrm{K}$, only $v = 2$ masers occur in the region of kinetic temperature $1100\,\mathrm{K} < T_\mathrm{k} < 1500\,\mathrm{K}$ and density $n(\mathrm{H_2}) > 2 \times 10^{10}\,\mathrm{cm}^3$. Inversely, with the same set of parameters, T_k of 1400 K and $n(\mathrm{H_2})$ of $10^{10}\,\mathrm{cm}^3$ give $500\,\mathrm{K} < T_\mathrm{d}^\mathrm{off} < 700\,\mathrm{K}$, where $T_\mathrm{d}^\mathrm{off}$ is the dust temperature at which the $v = 1$ masers disappear and $v = 2$ masers might remain if $T_\mathrm{d} > T_\mathrm{d}^\mathrm{off}$. If T_d is heated mainly by a central star of $L \sim 10^4 L_\odot$, the region of $T_\mathrm{d}^\mathrm{off} \sim 600\,\mathrm{K}$ is at 25 AU, which

is consistent with our observation (assuming radiative equilibrium, $L = \sigma T^4 4\pi r^2$).

Reid et al. (2007) imaged Source I at 43 GHz with VLA, and found disk-like continuum emission. They argued that the emission could be modeled by either a collisional-ionized disk heated by local heating due to accretion (Model B) as well as the central star or photo-ionized disk (Model C). Above all, Model B well explains the observed continuum emission and the SiO masing region. At 20 AU from the center, where $T_{\rm d} \sim 700$ K assuming radiation equilibrium, the estimated temperature is 1800 K and the density is 4×10^{12} cm^{-3} with the parameters of model B. For a distance of 30 AU from the center, where $T_{\rm d} \sim 550$ K, the temperature will be 1500 K and the density is 2×10^{12} cm^{-3}. Comparing these estimations to the models mentioned above, the SiO masing region has a lower temperature and a lower density of two orders of magnitude than those of compact emission, estimated by Reid et al. (2007). Since Model B suggests a the thick disk and that the SiO masers trace the outer edge of the disk, these differences in the temperature and the density may be reasonable.

As stated above, the physical properties estimated from a comparison of our observations with the pumping models suggest that the two vibrational transitions occur in the regions of a distinct physical parameter, and the ionized disk model of Source I proposed by Reid et al. (2007) can provide the required high temperature and density. However, most of models assumed spherical symmetry, which is contrary to the observed outflow/disk. Thus, further detailed modeling based on our results that the SiO masers are proposed to be excited in the rotating circumstellar disk around Source I should be required in order to account for the pumping mechanism of the SiO masers. In addition, it will be quite interesting to conduct VLBI observations of SiO masers in higher frequency transitions in the future. Cho et al. (1999) found that $v = 1$ $J = 2$–1 and $v = 2$ $J = 3$–2 masers show a double-peaked spectra similar to that of $v = 1$, 2 $J = 1$–0 masers. They expected that these masers lie closer to Source I, but, in the VLBI observation, $v = 1$ $J = 2$–1 masers are found in a region slightly farther than the $v = 1$ $J = 1$–0 in Orion-KL, (Doeleman et al. 2004) against the expectation that the high-J or high-v masers lie closer to the star. Therefore, multi-line imaging of this region could reveal a special nature of SiO masers in Orion-KL and will allow us to trace the physics and dynamics of this region.

5. Conclusion

We made multi-epoch phase-referencing VLBI observations of the SiO masers associated with Orion-KL with VERA. From these data, we found that Orion-KL is at a distance of 418 ± 6 pc. This result gives the distance to Orion-KL with the highest accuracy among the existing trigonometric parallax measurements. We imaged SiO $v = 1$ $J = 1$–0 and $v = 2$ $J = 1$–0 maser emissions in Orion-KL and compared the absolute positions of the maser features with that of Source I. The maser emissions show an X-shaped distribution centered at Source I, also, the radial velocities of the maser features tend to decrease with the distance from the central star, Source I. This suggests that the SiO masers lie in the rotating materials associated with an accretion disk, rather than a decelerating outflow.

In our observations, it has been confirmed that there is a positional offset of ~ 20 mas between the SiO $v = 2$ emissions and the SiO $v = 1$ emissions. This offset indicates that the two vibrational transitions occur in the regions of distinct physical parameters. However, further detailed modeling and high-resolution observations of higher frequency transitions will be required to understand the maser pumping mechanism as well as the physics and dynamics of massive star formation in the very vicinity of the central object.

We are grateful to an anonymous referee for valuable comments and suggestions. We also thank to the staff members of all the VERA stations for their assistance in the observations.

References

Bally, J., & Zinnecker, H. 2005, AJ, 129, 2281
Bujarrabal, V. 1994, A&A, 285, 953
Cho, S.-H., Chung, H.-S., Kim, H.-R., Kim, H.-G., & Roh, D.-G. 1999, AJ, 117, 1485
Cohen, R. J., Gasiprong, N., Meaburn, J., & Graham, M. F. 2006, MNRAS, 367, 541
Deguchi, S., & Nguyen-Quang-Rieu 1983, A&A, 117, 314
Doeleman, S. S., Lonsdale, C. J., Kondratko, P. T., & Predmore, C. R. 2004, ApJ, 607, 361
Doeleman, S. S., Lonsdale, C. J., & Pelkey, S. 1999, ApJ, 510, L55
Elitzur, M. 1980, ApJ, 240, 553
Elitzur, M. 1982, ApJ, 262, 189
Gaume, R. A., Wilson, T. L., Vrba, F. J., Johnston, K. J., & Schmid-Burgk, J. 1998, ApJ, 493, 940
Genzel, R., Reid, M. J., Moran, J. M., & Downes, D. 1981, ApJ, 244, 884
Genzel, R., & Stutzki, J. 1989, ARA&A, 27, 41
Gezari, D. Y. 1992, ApJ, 396, L43
Gezari, D. Y., Backman, D. E., & Werner, M. W. 1998, ApJ, 509, 283
Gomez, L., Rodríguez, L. F., Loinard, L., Lizano, S., Poveda, A., & Allen, C. 2005, ApJ, 635, 1166
Greenhill, L. J., Gwinn, C. R., Schwartz, C., Moran, J. M. & Diamond, P. J. 1998, Nature, 396, 650
Greenhill, L. J., Reid, M. J., Chandler, C. J., Diamond, P. J. & Elitzur, M. 2004, in IAU Symp. 221, Star Formation at High Angular Resolution, ed. M. Burton , R. Jayawardhana, & T. Bourke, 155
Hirota, T., et al. 2007, PASJ, 59, 897
Hirota, T., et al. 2008, PASJ, 60, 37
Honma, M., et al. 2003, PASJ, 55, L57
Honma, M., et al. 2007, PASJ, 59, 889
Honma, M., Tamura, Y., & Reid, M. J. 2008, PASJ, 60, 951
Imai, H., et al. 2007, PASJ, 59, 1107
Kawaguchi, N., Sasao, T., & Manabe, S. 2000, Proc. SPIE, 4015, 544
Kobayashi, H., et al. 2008, in IAU Symp. 248, A Giant Step: from Milli- to Micro-arcsecond Astrometry, ed. W. Jin, I. Platais, & M. A. C. Perryman (Cambridge UK: CUP), 148
Ma, C., et al. 1998, AJ, 116, 516

Matthews, L. D., Goddi, C., Greenhill, L. J., Chandler, C. J., Reid, M. J., & Humphreys, E. M. L. 2007, in IAU Symp. 242, Astrophysical Masers and their Environments, ed. J. M. Chapman & W. A. Baan (Cambridge UK: CUP), 130
Menten, K. M., & Reid, M. J. 1995, ApJ, 445, L157
Menten, K. M., Reid, M. J., Forbrich, J., & Brunthaler, A. 2007, A&A, 474, 515
Miyoshi, M., Matsumoto, K., Kameno, S., Takaba, H., & Iwata, T. 1994, Nature, 371, 395
Morita, K., Hasegawa, T., Ukita, N., Okumura, S. K., & Ishiguro, M. 1992, PASJ, 44, 373
Petrov, L., Hirota, T., Honma, M., Shibata, K. M., Jike, T., & Kobayashi, H. 2007, AJ, 133, 2487
Plambeck, R. L., Wright, M. C. H., & Carlstrom, J. E. 1990, ApJ, 348, L65
Reid, M. J., Menten, K. M., Greenhill, L. J., & Chandler, C. J. 2007, ApJ, 664, 950
Rodríguez, L. F., Poveda, A., Lizano, S., & Allen, C. 2005, ApJ, 627, L65
Sandstrom, K. M., Peek, J. E. G., Bower, G. C., Bolatto, A. D., & Plambeck, R. L. 2007, ApJ, 667, 1161
Soria-Ruiz, R., Colomer, F., Alcolea, J., Desmurs, J. F., Bujarrabal, V., Marvel, K. M., Diamond, P. J., & Boboltz, D. 2005, in ASP Conf. Ser. 340, Future Directions in High Resolution Astronomy: The 10th anniversary of the VLBA, ed. J. Romney & M. J. Reid (San Francisco: Astronomical Society of the Pacific), 384
Wright, M. C. H., Carlstrom, J. E., Plambeck, R. L., & Welch, W. J. 1990, AJ, 99, 1299
Yi, J., Booth, R. S., Conway, J. E., & Diamond, P. J. 2005, A&A, 432, 531
Zeng, Q., Sun, J., & Lou, G. F. 1987, A&A, 172, 299